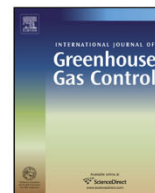# Dynamics of rising CO^2 bubble plumes in the QICS field experiment: part 2; modelling.

DEWAR, M., SELLAMI, N., CHEN, B.

2015

Dynamics of rising CO_2 bubble plumes in the QICS field experiment Part 2 – Modelling

Marius Dewar, Nazmi Sellami, Baixin Chen *

Institute of Mechanical, Process and Energy Engineering, Heriot-Watt University, Riccarton, Edinburgh EH14 4AS, Scotland, United Kingdom

ARTICLE INFO

ABSTRACT

An oceanic two-phase plume model is developed to include bubble size distribution and bubble inter-actions, applied to the prediction of CO_2 bubble plume and CO_2 solution dynamics observed from the recent QICS field experiment in the Scottish sea at Ardmucknish Bay. Observations show bubbles form at between 2 and 12 mm in diameter, where the inclusion of the interactions within the simulations brings results of bubble plumes closer to that of the experiment. Under a given leakage flux, simulations show that the bubble size affects the maximum pCO_2 dissolved in the water column, while the bubble interactions affect the vertical bubble distribution. The maximum modelled pCO_2 increases from a background 360 μatm to 400, 427 and 443 μatm as CO_2 injection rates increase from 80, 170 to 208 kg/day respectively at low tide. An increase of the leakage rate to 100% of the injection rate shows the maximum pCO_2 could be 713 μatm, approaching the mean pCO_2 observed of 740 μatm during the high leakage component of the experiment, suggesting that the flux may be greater than estimated due to the varied flux and activity across the pockmarks during the leakages.

1. Introduction

The greatest concern on performing carbon capture and storage (CCS) is the risk and impacts of any potential CO_2 leakage from storage reservoirs into the water column, marine environment and atmosphere (IEA Greenhouse Gas R&D Programme (IEA GHG), 2008). In order to study the effects of a potential leak from CCS on the marine environment, the quantifying and monitoring potential ecosystem impacts of geological carbon storage project (QICS) was launched to design and test monitoring methods, gain valuable experimental data, and develop models to determine the fate of the leaked CO_2, where sufficient understanding of CO_2 bubble rising and dissolution characteristics is necessary to determine the changes in dissolve inorganic carbon (DIC), pH and seawater pCO_2.

Two-phase or two-fluid CO_2 droplet plume models (Chen et al., 2003; Alendal and Drange, 2001; Sato and Sato, 2002) have been developed attempting to predict the physicochemical impacts of direct injection of CO_2 into middle depth of the ocean. In the development of the bubbly flow numerical model to simulate the fate of CO_2 and CO_2 solution plumes, such as those experienced within

QICS field experiment, the size of the bubbles forming under a certain of leakage flux has previously been found to impact greatly on both the dissolution rate through mass transfer and the rising height of the bubble plume (Dewar et al., 2013a,b; Kano et al., 2009; Nguyen et al., 2013). Wu et al. (1998) state that the impact is due to the mass, momentum and energy exchanges; defined using a geometrical factor from the bubble volume V_i and cross sectional area A_i through use of the interfacial area concentration $a^{-V} = V_i/A_i$ (Ishii and Mishima, 1980). This geometrical parameter can be redefined through use of the equivalent diameter of the bubble d_{eq}.

$$d_{eq} = \frac{6}{a_i^{-V}} \qquad (1)$$

In previous work by Dewar et al. (2013a,b), the bubble phase flow is modelled on an Eulerian scheme, where the flow of bubbles through a region is analysed by considering the void fraction α and number density n (number of bubbles per unit volume) in addition to the Navier–Stokes based momentum equations for velocity. From this, the mean bubble equivalent diameter in a given volume may be defined as:

$$\bar{d}_{eq} = \sqrt[3]{\frac{6\alpha}{\pi n}} \qquad (2)$$

A number of factors can affect the bubble size, the geometry (the deformation of bubbles from sphere), dissolution through

* Corresponding author. Tel.: +44 131 451 4305.
  E-mail address: b.chen@hw.ac.uk (B. Chen).
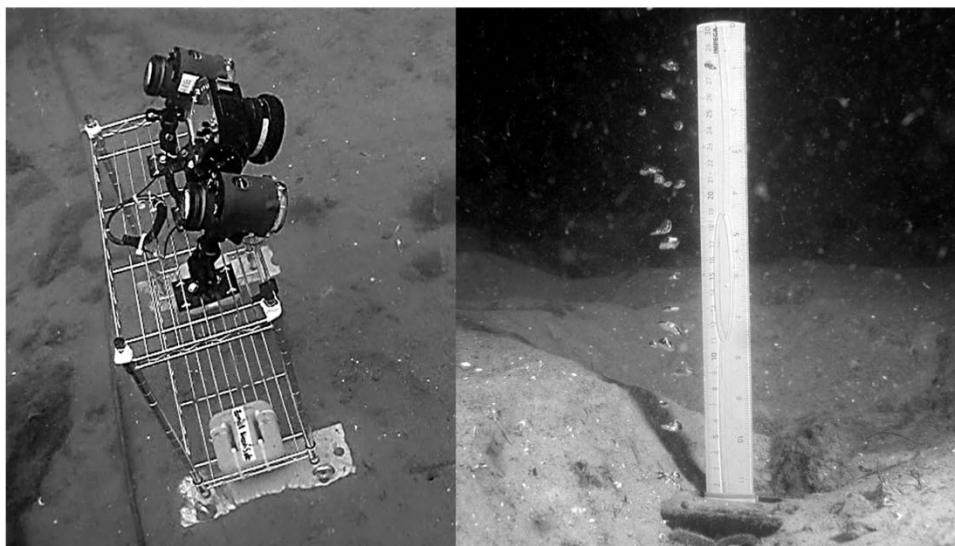
Fig. 1. Experimental equipment, Canon EOS 5D Mark II time-lapse camera on the left, ruler as scale with CO_2 bubbles rising freely from the sediments (enhanced contrast to highlight the bubbles).

mass transfer (volume reduction) and decreasing pressure gradients (volume expansion). But also the breakup and coalescence of bubbles during the formation, rise and dispersion of a bubble plume will have an effect on the size and fate of the bubbles. Mass transfer and density expansions have previously been modelled in many studies, however there are far less data and modelling on coalescence and breakup dynamics required to predict the bubble interactions in plumes (Hibiki and Ishii, 2000a).

The main aims of this study are to develop a suitable sub-model of bubble interactions in a free rising plume by analysing existing models in a different setting against the data collected (the details can be found in part one of this study (Sellami et al., 2015)) from the QICS in situ leakage experiment to predict the fate of the bubble plume witnessed; and to investigate the mechanism by comparing the measured physiochemical impacts of the leakage on the water column in terms of the bubble plume and pCO_2, with those predicted during experiment CO_2 injection rates into the sediments of 80 kg/day, 170 kg/day and 208 kg/day.

2. The QICS project experiment data of leaked bubbles and pCO_2

Quantifying and monitoring potential ecosystem impacts of geological carbon storage (QICS) is a project funded through the UK Research Councils with the aim of improving the understanding on the potential impacts of a leakage from carbon dioxide geological storage on the ecosystem and to investigate a variety of techniques and methods that may be suitable for monitoring leakage. It also aims to predict on a small scale, the effect of leakage through a unique real world release of CO_2 beneath the sea-floor on the marine environment, to further investigate the ecosystem impact and recovery.

The experiment involved drilling a narrow borehole from land, terminating in unconsolidated sediments 10 m below the sea floor, with 9–12 m head of seawater in a semi enclosed bay. The release was carried out in May–June 2012, continuing for 37 days with a cumulative release of 4.2 tonnes of CO_2. Leaked CO_2 bubbles freely rising in the first 30 cm from the sediments into the water column are observed and tracked through analysing the video clips from three select pockmarks locations utilising a HDTV Canon EOS 5D Mark II camera and a ruler aligned with the CO_2 bubble plume as a

reference dimension as seen in Fig. 1. This limits the experimental data to the first 30 cm in the water column. Therefore data such as the rise height of the bubbles is observational data rather than quantitative, where bubbles of an unmeasurable size (very small) were noticed to reach the water surface during low tide.

The distribution of the bubbles leaked from the sediments is measured, along with the observation of interactions such as breakup of the CO_2 bubbles as seen in Fig. 2, which reduces the bubble size and therefore velocity, or coalescence between two CO_2 bubbles to give birth to a larger CO_2 bubble with a higher velocity.

In the experiment upwards of 35 pockmarks were formed, where video sets only captured three select locations, therefore the work is based only on the data available and provides a limitation on the applicability of the data gained to extrapolate through to the full experiment in open waters. Some inaccuracies occurred by nature of the field experiment, such as the lack of measurements in three dimensions due to a single camera, noise from particles in the seawater, and both focal and motion blur from the fast moving three dimensional bubbles. If the resolution is also taken into account on top of these uncertainties an error of ±0.5 mm for the bubble size measurement is accumulated. Greene and Wilson (2012) suggest that an improvement on gaining the initial bubble distribution would be through an acoustic method, investigating initial bubble sizes with a greater accuracy than imaging methods, however this would provide no data on the bubble interactions.

2.1. Experiment bubble shapes and size distribution

The bubble size (measured by the equivalent diameter, d_{eq}) distribution leaving the sediments was observed, with 50% of the measured CO_2 bubbles having a diameter of between 6.5 mm and 9.0 mm, with only a low quantity (<1.5%) of small and large bubbles (diameter < 0.4 cm and diameter > 1.1 cm respectively) as shown in Fig. 3. This distribution has been applied in the modelling simulations by setting the initial bubble size leaked from sediments, which will be discussed in Section 4.2. It is also observed from QICS experiment that the bubbles are in a variety of shapes, smaller sphere, ellipse and ellipsoidal cups, as shown inside of Fig. 3. The effects of bubble shapes on dynamics of bubble mass and momentum exchange with the seawater have been modelled and described in detail and found in the previous study by Dewar et al. (2013a).
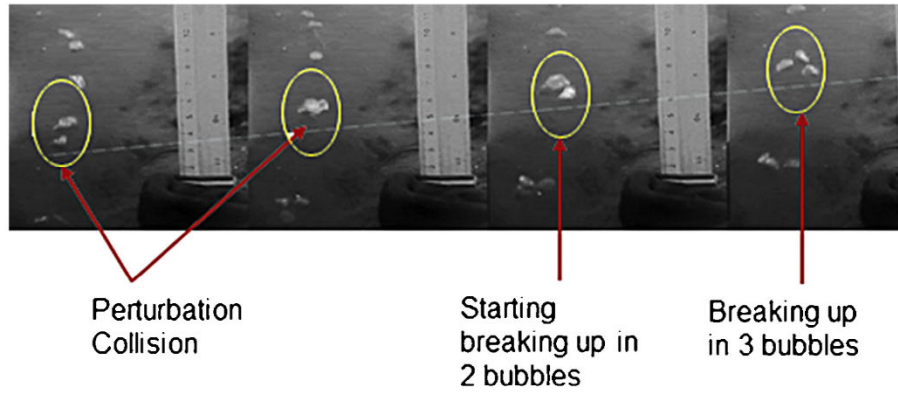
Fig. 2. Bubble breakup, where two bubbles collide, but fail to coalesce. However, the collision creates an instability forcing the larger bubble to break in two.
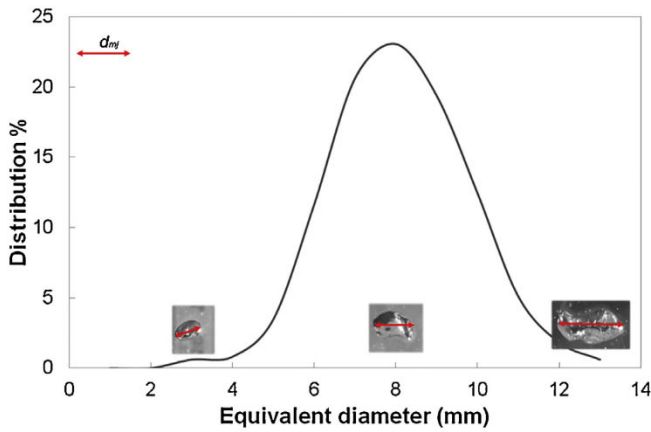

Fig. 3. Bubble size distribution measured as the bubbles leave the sediments.

2.2. Breakup and coalescence

Breakup frequency is an important parameter to predict the dynamics of bubbles in a plume. As the smaller bubbles break up from a relatively large bubble, they will rise at a lower rate and dissolve far quicker, greatly affecting the overall structure of the plumes. In general, the breakup of freely rising bubbles could be identified by using the non-dimensional Eötvös number Eo, the ratio of buoyancy force by the surface tension force, and Reynolds number Re, the ratio of inertial force to viscous force, through use of the equivalent diameter, d_{eq}. It was found from the experiment data analysis, as reported in part one of the paper (Sellami et al., 2015), that bubbles that break up could not be differentiated from those that do not if the equivalent diameter, d_{eq} was used to define the Eötvös and Reynolds numbers. However, from the experiment data analysis it is identified that the bubble breakup can be indicated by using large major axis dimension, d_{mj}, instead the equivalent diameter, d_{eq}, as the length scale of Eötvös number, which is applied to this study by using the correlation between the two dimensions developed from the QICS experiment data

$$d_{mj} = 1.82d_{eq} - 0.4 \quad (mm) \qquad (3)$$

The frequency of bubble break up was detected as nine in every 354 new bubbles forming from the leakage location, from QICS experimental findings.

Coalescence between CO_2 bubbles has been recorded at a frequency of 2.5 Hz in the first 30 cm above the sea floor. When the bubbles coalesce, they form a larger bubble that will take longer to dissolve in the seawater. The frequency is applied in the examination of existing sub-models to describe bubble coalescence effects in the development of the two plumes, including the determination of the height that the bubbles can reach before dissolution.

2.3. pCO₂ and leakage rate measurements

Measurements of pCO_2 were taken in the later stages of the experiment at 30 cm from the seabed, along with estimates on the leakage rate (Blackford, 2014). On day 30 (at the injection rate of 170 kg/day), a mean pCO_2 of 390–400 μatm was measured during both high and low tide, rising from a background of 360 μatm. On days 32–36, where the injection rate was increased to the maximum (208 kg/day), the pCO_2 varied, rising from 390 μatm to a peak of 1500 μatm before settling back at around 500 μatm. Overall with a mean value of 740–750 μatm across the later stages of the gas injection in experiment during the high injection phase. The measured leakage rate (the leaked bubbles from sediments) from day 33 is 32.1 kg/day, with acoustic measurements giving similar leakage estimates at low tide. The observation data are used in this study for model validation and simulation analysis, which are discussed in Sections 4 and 5.

3. Modelling of the bubble interactions of QICS experiment

In developing the bubble interaction models through coalescence and breakup, consideration of the distribution of bubble sizes and the ocean turbulence interactions with the bubbles is vital (Nguyen et al., 2013). In bubbly flow, it has been shown in Section 2 that collisions can cause bubbles to breakup and/or coalesce, which further affect bubble size distributions and then alter both bubble and plume dynamics (Dewar et al., 2013a,b). The main driving dynamics that make bubble coalescence occur can be described through random coalescence through turbulent flows, coalescence through laminar shear forces, and coalescence through wake entrainment. For bubble breakup the main driving mechanisms are bubble collisions with turbulent eddies, velocity gradients, large (cap) bubbles shearing smaller bubbles, and the complete breakup of large (cap) bubbles (Wu et al., 1998).

Mechanisms such as laminar shearing and interactions through velocity gradient are neglected from the models as they are not directly based upon the distribution of bubble parameters or void fraction (Wu et al., 1998). The coalescence through wake entrainment also occurs with large bubbles in cap or slug like structures within pipelines (Hibiki and Ishii, 2002), where Yao and Morel (2004) state that smaller spherical or ellipsoidal bubbles will repel each other. Considering the frequency of bubble interactions, ϑ, this leads to the relationships of the breakup frequency ϑ_b and

coalescence frequency ϑ_c, mainly due to the effects of turbulent eddies.

$$\vartheta = \vartheta_c - \vartheta_b \tag{4}$$

A number of models have been developed and reported in literature following the breakup and coalescence process within a pipeline setting (Wu et al., 1998; Hibiki and Ishii, 2000a,b, 2002; Nguyen et al., 2013; Ishii and Kim, 2001; Fu and Ishii, 2002; Sun et al., 2004; Yao and Morel, 2004), and a recent study on droplet formations from oil blowouts (Zhao et al., 2014). Care must be taken in the use of these models in bubbly plumes, as existing models were designed to simulate interactions in pipeline flow with turbulence at larger Reynolds numbers that affect the overall prediction. However Hibiki and Ishii (2000b) state that as the models are derived under the assumption of bubbles in an infinite space without taking into account the bubble interactions with the pipeline walls, the models could be appropriate for simulating open waters. Therefore, the existing models are examined with data from the QICS experiment, and then the selected models are applied to the experiment simulations.

Recent bubbly flow simulations (Chen et al., 2005b; Cheung et al., 2007) have had issues with the inclusion of coalescence models by Prince and Blanch (1990) and Luo and Svendsen (1996), where the models appear to exaggerate the rate of coalescence (Nguyen et al., 2013). Therefore later developed models are investigated within this study, although many refer back to the early work.

The bubble coalescence and break up can be defined through a term of efficiency η_k, the proportion of multi bubble collisions causing coalescence and break up, and a term for the collision frequency f_k of the bubbles,

$$\vartheta_k = \eta_k f_k \tag{5}$$

for coalescence, subscript $k = c$, and for break up, $k = b$ respectively.

3.1. Interaction (coalescence and breakup) efficiency

A number of models (Wu et al., 1998; Ishii and Kim, 2001; Fu and Ishii, 2002; Sun et al., 2004) consider the coalescence efficiency to be a constant, at range from 0.004 to 0.056, whereas others (Hibiki and Ishii, 2000a,b, 2002; Yao and Morel, 2004; Nguyen et al., 2013) base the coalescence efficiency on a model by Coulaloglou and Tavlarides (1977) to describe the quantity of coalescence occurrences in liquid/liquid dispersions, where the quantity of droplets that provide coalescence from a collision is predicted using an exponential of a time ratio of the time required to provide coalescence from film drainage, t_c, against the contact time between the bubbles, τ_c.

$$\eta_c = \exp\left(-\frac{t_c}{\tau_c}\right) \tag{6}$$

This was modified to gas/liquid dispersions through a thin film model, the time for coalescence of bubbles through film drainage and thinning is defined by Oolman and Blanch (1986a,b) and Prince and Blanch (1990). With the contact time for turbulent flows defined by Levich (1962), giving the overall coalescence efficiency as

$$\eta_c = \Gamma_{RC} \exp\left(-Kc\frac{\bar{\rho}^{1/2} d_{eq}^{5/6} \varepsilon^{1/3}}{\sigma^{1/2}}\right) \tag{7}$$

with σ as the surface tension and ε as the turbulent kinetic energy dissipation rate. Γ_{RC} and K_C are coefficients decided from experimental data. As found by Nguyen et al. (2013), the predicted efficiency can vary greatly depending on the use of the varied constants and coefficients (Γ_{RC}, K_C) for a set energy dissipation rate.

Both Γ_{RC} and K_C are suggested (Hibiki and Ishii, 2000a,b, 2002; Yao and Morel, 2004; Nguyen et al., 2013) being in a wide range, from 0.188 to 2.86 and 0.26 to 1.29 respectively. Nguyen et al. (2013) proposed to take the effects of bubble size into account by $K_C = 0.913/C^{2/3}$, with C as the coefficient of bubble size distribution and velocity.

Unlike the coalescence model, for breakup, all the models simulate the efficiency in the same manner, based on a model by Coulaloglou and Tavlarides (1977) using the ratio of energy required for a bubble to breakup $\bar{E}_B$, against the mean energy from a single turbulent eddy $\bar{e}_B$.

$$\eta_b \propto \exp\left(-\frac{\bar{E}_b}{\bar{e}_b}\right) \tag{8}$$

The ability of a bubble to resist the breakup is based on the surface tension (Prince and Blanch, 1990). Wu et al. (1998) considers the energy to be proportional to the squared velocity, and in turn the weber number $We = \rho_f u^2 d_{eq}/\sigma$. A critical weber number will occur providing the largest stable size of the bubble where inertial forces equal the tension maintaining the bubble without breaking (Prince and Blanch, 1990). The critical weber number value is merged with a constant K_b for clarity. As with the coalescence efficiency, there are differences in this term depending on the model in use, where discrepancies come from the adjustable coefficients and the choice of critical Weber number.

It is stated by Wu et al. (1998) that only eddies of a similar size to that of the bubble will be effective in breakup, with Hibiki and Ishii (2002) and Nguyen et al. (2013) describing that larger eddies move groups of bubbles with minimum interaction and smaller eddies unable to provide enough interacting energy to the bubble. Therefore the breakup efficiency is based on a bubble breaking up with an eddy of equivalent size giving the following relation:

$$\eta_b = \Gamma_b \exp\left(-\frac{K_b}{We}\right) \tag{9}$$

The two suggested breakup constant coefficients are Γ_b, from 0.021 to 1.6, and K_b, from 1.24 to 6.85 (Wu et al., 1998; Hibiki and Ishii, 2000a,b, 2002; Nguyen et al., 2013; Ishii and Kim, 2001; Fu and Ishii, 2002; Sun et al., 2004; Yao and Morel, 2004). However, Nguyen et al. (2013) proposed to take the effects of turbulence suppression into account by $K_b = 1.581/(1.0 - 0.1u')$, with u' defined as the turbulent velocity in relation to the mean velocity.

3.2. Collision frequency

The collision frequency is modelled on the basis of a prediction of the random collision rate. For coalescence, Wu et al. (1998) define it by the relative velocity and distance between two neighbouring bubbles, along with a probability function that the bubbles are moving towards one another.

$$f_c = \frac{n^2 \bar{u}' d_{eq}^2}{\left(\alpha_{max}^{1/3}\left(\alpha_{max}^{1/3} - \alpha^{1/3}\right)\right)} \left[1 - \exp\left(-3.0\frac{\left(\alpha_{max}^{1/3}\alpha^{1/3}\right)}{\left(\alpha_{max}^{1/3} - \alpha^{1/3}\right)}\right)\right] \tag{10}$$

However, the collision frequency for breakup is predicted in terms of the driving force from the turbulent eddy's inertia, and the tension force holding the bubble together

$$f_b = \frac{n_b \bar{u}'}{d_{eq}}\left(1 - \frac{We_{cr}}{We}\right)^{1/2} \tag{11}$$

Hibiki and Ishii (2000a,b, 2002) use the kinetic theory of ideal gas molecules, representing bubbles or turbulent eddies, to predict the frequency of collisions for both bubble coalescence and breakup.

$$f_c = \frac{\bar{u}'}{d_{eq}} \frac{\alpha}{(\alpha_{\max} - \alpha)} \tag{12.a}$$

$$f_b = \frac{\bar{u}'}{d_{eq}} \frac{(1 - \alpha)}{(\alpha_{\max} - \alpha)} \tag{12.b}$$

Yao and Morel (2004) and Nguyen et al. (2013) also use a kinetic theory, but suggest that the time for collision, along with the time between each collision is required to predict the frequency.

$$f_c = \frac{\varepsilon^{1/3}\alpha^2}{d_{eq}^{1/3}} \frac{1}{g(\alpha) + 1.922\alpha\sqrt{We/1.24}} \tag{13.a}$$

$$f_b = \frac{\varepsilon^{1/3}\alpha(1 - \alpha)^2}{d_{eq}^{1/3}} \frac{1}{1 + 0.42(1 - \alpha)\sqrt{We/1.24}} \tag{13.b}$$

with $g(\alpha)$ as a limiting factor as described by Yao and Morel (2004).

For the models of Eqs. (10)–(13), the maximum bubble void fractions $\alpha_{\max}$ were suggested (Wu et al., 1998; Hibiki and Ishii, 2000a,b, 2002; Nguyen et al., 2013; Ishii and Kim, 2001; Fu and Ishii, 2002; Sun et al., 2004; Yao and Morel, 2004) to be in the range between 0.52 and 0.8 for the coalescence collision frequency, and critical Weber numbers We_{cr} of 2.0–6.0 (Wu et al., 1998; Ishii and Kim, 2001; Fu and Ishii, 2002) and the maximum void fraction at a range of 0.52–0.741 (Hibiki and Ishii, 2000a,b, 2002; Nguyen et al., 2013; Yao and Morel, 2004) for the breakup collision frequency.

3.3. The turbulent kinetic energy dissipation rate

In this study, the law of the wall (Bradshaw and Huang, 1995) is adopted to predict the turbulent kinetic energy dissipation rate in the ocean bubbling plume through the mean current velocity, U_y,

$$\frac{U_y}{u_\tau} = \frac{1}{\kappa} \ln\left(\frac{u_\tau y}{\nu}\right) + C \tag{14}$$

with κ and C constants of 0.41 and 5.0 respectively from experimental data, ν is the seawater viscosity, and $u_\tau = \sqrt{\tau_w/\rho_f}$ is the friction velocity, with τ_w as the shear stress. The turbulent kinetic energy dissipation rate can be taken from the velocity fluctuations as

$$\varepsilon = \frac{(u'^2/2)^{3/2}}{d_{eq}} \tag{15}$$

3.4. Modelling of the QICS experiment interactions

Implementing the sub-models discussed in Sections 3.1 and 3.2 into the two-phase plume models, the coalescence frequency is found to vary with depth. From the simulation of the QICS experiment, the best matched results come from the sub-model proposed by Nguyen et al. (2013), Eq. (13.a). As shown in Fig. 4, it is found that some models over predict the coalescence near the sediments, such as that by Wu et al. (1998) and Yao and Morel (2004); and under prediction is found from the models by Hibiki and Ishii (2000a,b, 2002), Ishii and Kim (2001) and Fu and Ishii (2002).

The low depth over and under prediction from the sub-models by Wu et al. (1998) and Hibiki and Ishii (2000a,b, 2002) can be explained, in general, through the fact that the constants of the models were set from fluids other than CO_2-seawater. It had been suggested that a constant void fraction may be employed to predict the bubble coalescence frequency within a pipe flow. However, in the open waters, the local void fraction varies and must be determined visually from the bubble plume, which cannot be a constant parameter.

Table 1
The list of source terms for the dependent variable in the governing equation, where P is the dynamic pressure, μ is the turbulent viscosity, and g is gravity.

Dependant variable ϕ_k	Source terms $q_{k,\phi}$
$\bar{u}_{1,i}$	$\bar{\alpha}(\bar{\rho}_2 - \bar{\rho}_1)g - \dot{F}$
$\bar{\alpha}$	$-\dot{w}_{CO_2}$
$\frac{\bar{n}_d}{\bar{\rho}_1}$	$-\frac{\vartheta}{\bar{V}}$
$\bar{u}_{2,i}$	$-\frac{\partial P}{\partial x_i} + \frac{\partial}{\partial x_j}\left(\mu\frac{\partial u_{2,i}}{\partial x_j}\right) - \hat{\alpha}(\bar{\rho}_2 - \bar{\rho}_0)g + \dot{F}$
$\lfloor \bar{T}, \bar{S}, \bar{Y}_d \rfloor$	$\lfloor 0, 0, \dot{w}_{CO_2} \rfloor$

Nguyen et al. (2013) state that their model is an improvement on the model by Yao and Morel (2004) due to the bubble distribution and turbulence suppression taken into account after collisions which may explain why the frequency is a closer match to the experimental data, with a minimum coalescence frequency in the first few centimetres, rising to same order of the experimental data, reaching a peak of 2.75 Hz at 7.0 cm height from the sediments, before starting to decrease with greater distances from the seafloor.

Although the breakup is witnessed to be of orders lower than the coalescence within the QICS experiment, it was observed from video recorded data. However all the existing models, based on the concept of turbulent eddy interactions, either failed to predict breakup frequencies or became unstable due to the low weber numbers. The reason is that the breakup in the experiment is considered to be not from the turbulent eddies, but due to the larger cap like bubbles at high Eötvös numbers as mentioned in part one of the paper (Sellami et al., 2015). The turbulent breakup model by Nguyen et al. (2013), Eq. (13.b) is however to be included in the two phase model simulation along with a statistical large cap breakup model taken from the experimental data.

4. Modelling of the plume dynamics of the QICS experiment

4.1. Governing equations

The numerical two phase model used to simulate the leakage plume dynamics within the QICS experiment is based upon the Eulerian–Eulerian droplet model by Chen et al. (2003, 2005a), was further developed for use with bubble simulations by Dewar et al. (2013a,b). The governing equations of the conservation of mass and momentum can be expressed as

$$\frac{\partial \bar{\rho}_k\phi_k}{\partial t} + \frac{\partial \bar{\rho}_k\phi_k\bar{u}_{k,j}}{\partial x_j} = q_{k,\phi} \tag{16}$$

where $k = 1, 2$ indicates bubble plume or seawater, with the dependant variables $\phi_1 = [\bar{u}_{1,i}, \bar{\alpha}, \bar{n}_d]$ and $\phi_1 = [\bar{u}_{2,i}, \bar{T}, \bar{S}, \bar{Y}_d]$, respectively. For seawater, T represents temperature, S salinity, and Y_d, the mass fraction of dissolved CO_2 in water. t is the time, x the spatial coordinate, and the directional vectors are represented through the subscript 'i'. The source terms $q_{k,\phi}$ describing the mass and momentum exchanges between two plumes can be found in Table 1. Calculations of all fluid properties such as densities and turbulent diffusivities are as modelled in Dewar et al. (2013a,b) based on data provided from the experiment in Section 2. Due to the short time period for plume development, the thermodynamic equilibrium is applied to the simulation of bubbles due to the vast volume of the waters and small volume of the leaked bubbles.

The sub-models for the mass and momentum exchange terms are as follows:

$$\dot{w}_{co_2} = (6\bar{\alpha})^{1/3}(\pi\bar{n})^{2/3}ShD_f(C_s - C_0) \tag{17}$$

for the mass transfer from CO_2 dissolution through the Sherwood number, Sh, used to calculate the effective mass transfer coefficient, k, as defined by Zheng and Yapa (2002), $Sh = d_{eq}k/D_f$ and D_f is
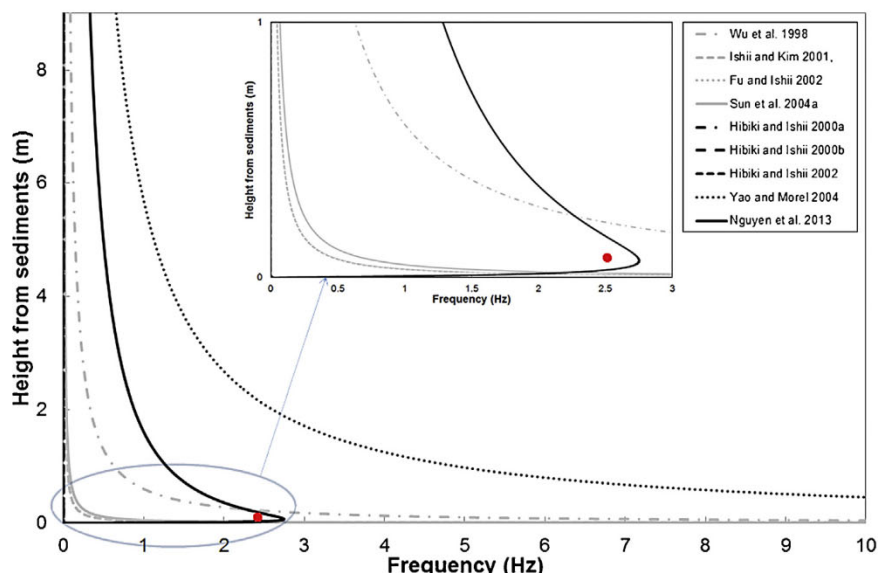
Fig. 4. Coalescence frequency models, with the red point showing the experimental findings. (For interpretation of the references to color in this figure legend, the reader is referred to the web version of this article.)

the CO_2 diffusivity, C_s is the CO_2 solubility and C_0 is the seawater background CO_2 concentration.

$$\dot{F} = 0.75 \left(\frac{\pi}{6.0} \right)^{1/3} \rho_1 \bar{\alpha}^{2/3} \bar{n}^{1/3} C_d |\bar{u}_{2j} - \bar{u}_{1j}| (\bar{u}_{2j} - \bar{u}_{1j}) \qquad (18)$$

for the momentum exchange term through the drag force between the bubble and the seawater, where C_d is the drag coefficient, for which, the model proposed by Bozzano and Dente (2001) is found to be the best matched model to the QICS experimental data as described in part one of the paper. The effects of bubble interactions are predicted by the changes in bubble number density at a rate of ϑ which is modelled from Eq. (4).

4.2. Model and simulation settings

The computational domain is set to be 50 m × 50 m × 9.5 m, with an equidistant grid of 298 × 298 × 23, giving a grid size in the horizontal directions as 16.78 cm, 16.78 cm, and 41.3 cm in the vertical direction. The grid size is considered to be approximately the size of the pockmarks, meanwhile is designed to predict the effects of small scale leakage from multiple separate pockmarks and the local impacts on the marine environment. Numerical simulations show that the modelled time step of 1.5 s can guarantee the numerical stability. Results are monitored and checked every 15 min of simulated time, by which the data from modelling plumes can be analysed and investigated, including when steady state is being approached.

In situ measurements taken from the leakage locations are used to set and calibrate the model. The simulations are performed to predict the plumes generated on the morning of the 12th of June 2012, during a mid-injection part of the experiment when the bubble plumes were filmed. The seawater data recorded are at a temperature of 10.7 °C, salinity of 34.7, with currents varying between −5 and +5 cm/s in the horizontal plane and the vertical current set as 0.0 cm/s. According to the experiment observations, the water depth of the model simulations is set with low and high tides of 9 m and 12 m respectively. The initial conditions are set for each simulation, with the seawater temperature, salinity, background pH and pCO_2 as recorded within the experiment shown above. The depth providing the pressure of the seawater, together with temperature and salinity, the densities of seawater and CO_2

are predicted from the international equation of state (Unesco, 1981) and by the data table (Ito, 1984), respectively. The increase in density of the dispersed CO_2-seawater solution, driving the CO_2 enriched plume descend, has been estimated from the dissolved CO_2 mass fraction using the experimental correlation by Song et al. (2005). The model small-scale ocean is numerically spun up by the observation data to a steady state before releasing the leaked CO_2 bubbles into the computation domain through the grids where the pockmarks are located. The control background pH level was 8.05–8.1, with a pCO_2 of 360 μatm.

To simulate the CO_2 release experiments, the bubbles are released into the constructed small-scale ocean through the location of the pockmarks at the initial diameter, randomly taken from the bubble size distributions, as shown in Fig. 3, both periodically and spatially as shown in Fig. 5.

The boundary conditions are set with the seabed as a non-slip closed-wall boundary, except for CO_2 bubbles at the leakage pockmarks, where the inlet boundary provides the means to release CO_2 bubbles for equations of gas bubble velocity, void fraction and number density. The upside boundary, towards the sea surface is considered a free surface boundary with no mass transfer for seawater. Bubbles reaching to the sea surface will be decided to release to the atmosphere in the next time step, meanwhile the uptake of CO_2 from atmosphere to the seawater is considered to be negligibly small within the time scale of the simulations.

The horizontal boundary conditions for spun-up the model ocean are updated periodically as a continuous flow in the direction of the seawater. Having released the CO_2, the inlet boundaries are kept with those of the model ocean, while the outlet boundary is setting by mass continuity using 3rd order differential scheme. To ensure numerical stability, the computation domain is tested to be sufficiently large to mitigate the effects of plumes of dissolved CO_2 and bubbles on the boundaries within the timeframe of the simulation.

5. QICS experiment simulation results and discussion

The first modelling case is designed to simulate the QICS experiment leakage at low tide and high injection rate of 208 kg/day providing a sediment leakage rate of 31.2 kg/day, for which the effects of bubble interactions on the plume development are
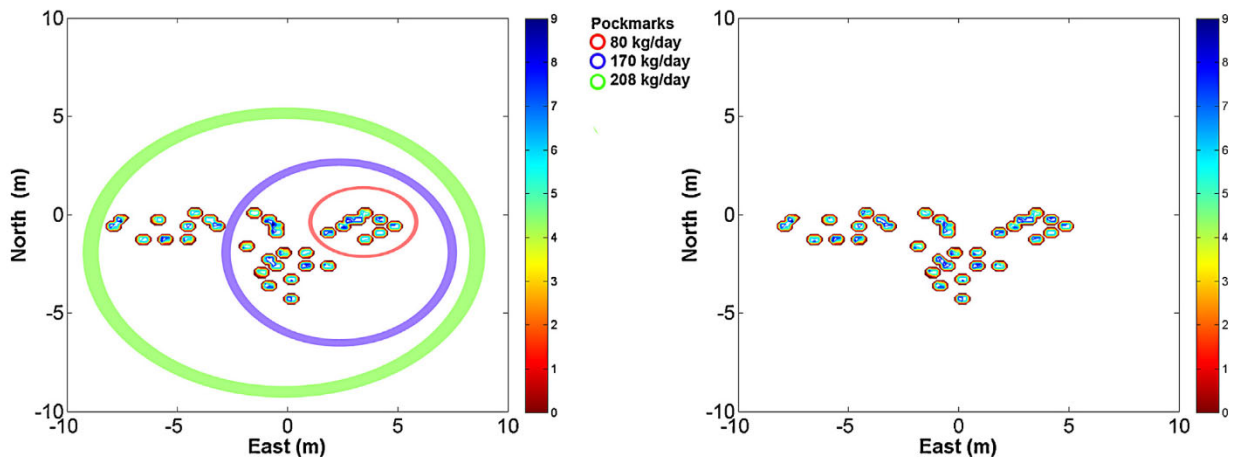
Fig. 5. The pockmark locations active at each leakage rate, with the initial bubble diameter (mm) shown by the colour map, where 10, 25 and 35 active pockmarks are suggested during the leakage rates of 80, 170 and 208 kg/day. (A) 15 min after leaking CO_2 into the ocean and (B) 30 min after leaking CO_2 into the ocean at leakage rate of 208 kg/day.

examined. The impacts of the leaked CO_2 on the QICS experiment waters for the period from the start to the end of the injection are simulated as the second case study to check the affected areas and the changes in pCO_2 of seawater. The final study is designed at low tide, as the presumed worst cases for the future experiments and diagnostics of the leakage mechanisms, where the leakage rate is set to 100% of the injection rate of 208 kg/day.

5.1. The leaked bubble plumes and the pCO_2 at a low tide

The modelling simulations of the first case predict that the leaked CO_2 bubbles visually ascend up to 8.8 m from the seabed before being considered completely dissolved (model set at $d_e < 0.01$ mm) when the bubble interactions are neglected as shown in Fig. 6A. The data are recorded from the simulation 4 h after the leakage starts when the simulation plumes have reached a semi-steady state, where the maximum pCO_2 settles at a constant value and the rate of change of the mean pCO_2 within the grid of pockmarks reduces to >1% of the initial rate of change, with minor fluctuations due to the changes in current. In such a simulation, the maximum bubble diameter is recorded as 8.3 mm, with a mean bubble diameter of 1.37 mm. However, when including the bubble interaction models, the bubble size increases in the first few centimetres through coalescence, before shrinking as dissolution takes over. Therefore the visible bubble plume ascends as shown in Fig. 6. B), almost approaching the surface, where undissolved bubbles were observed from the QICS experiment at low tide (Blackford, 2014). The mean bubble diameter increases to 1.41 mm, where the larger bubbles can ascend further in the water column, with a maximum bubble size of 9.8 mm.

There are a number of considerations that will affect the bubble plume simulations. The minimum bubble size that can be numerically modelled is 0.01 mm, therefore smaller bubbles may rise further. The effect from vertical current forcing (assumed to be 0 cm/s in the simulation), will be generated by tidal waves in the experiment, especially in the shallow water regions. The initial bubble size distribution, which is employed from experiment observations, is the data observed from three pockmarks, where there could be some larger bubbles that may occur from the other thirty-two pockmarks during the leakage. To investigate the mechanism of fate of an individual bubble with those in a plume, a free rising model of an individual bubble is applied to the QICS experiment in a quiescent ocean, and found, as shown in Fig. 7, that individual bubbles with a diameter smaller than 14.0 mm will completely dissolve before reaching the water surface. In comparison with the results from plume modelling (Fig. 6B), where the

bubbles with initial diameter of about 10 mm could almost manage to migrate to the water surface, it can be understood that the bubble interactions in the plume, the vertical current generated by the plume, and the reduction of dissolution rate due to the surrounding CO_2 concentration in the plume affect the fate of bubbles, providing differences with that of individual bubbles. From this result, it can be assumed that the largest bubbles leaked from the different pockmarks could be at a range of 10–14 mm in diameter from the QICS experiment sediments. This also highlights the effect of plume dynamics on bubble motion and dissolution providing a greater rise height of the gas bubbles in the experiment and plume model.

The reconstruction of the bubble size distribution through bubble interactions also provides an improvement on the distribution of the CO_2 solution plume, indicated by the pCO_2 levels shown in Fig. 8A without bubble interactions and Fig. 8B with interactions. The simulations show that with interactions, the maximum pCO_2 of the seawater slightly decreases from 445 μatm (Fig. 8A) to 443 μatm (Fig. 8B). As the dissolution is more distributed with the larger bubbles forming through the interactions, the entire dissolution rate is reduced, providing the lower levels of pCO_2 in the seawater. In comparison with the observation data, a mean pCO_2 of 390–400 μatm, increasing up to 1500 μatm, before reducing back to similar levels between 400 and 500 μatm (Blackford, 2014), it has been noted that the bubble interactions in such dilute plumes seem playing an insignificant role on creation of pCO_2 plumes, however, the difference distinguished from the models with and without including the bubble interactions indicates that the model including the bubble interactions can provide better results and has the potential to be applied to simulate the dense bubble plumes.

From these simulations, it is confirmed that at the level of pCO_2 from the QICS experiment, there should be a negligible impact on the marine environment, where accumulated experimental data according to the biological impact investigations (Gibson et al., 2011) shows that a pCO_2 of 1000 μatm is required to have an effect on marine larvae, embryos and juveniles, with effects dependant on the species, where there is an increase in mortality rates, especially in smaller invertebrates. Although in the experiment, this pCO_2 was exceeded, going to up to 1500 μatm, this was very localised to directly above the leakage pockmarks.

5.2. The impacts of leaked CO_2 on seawater from the QICS experiment

A full simulation of the QICS experiment at low tide has been implemented in the model by taking three of the injection rates (Fig. 9A), at the early, middle and late stages of the experiment
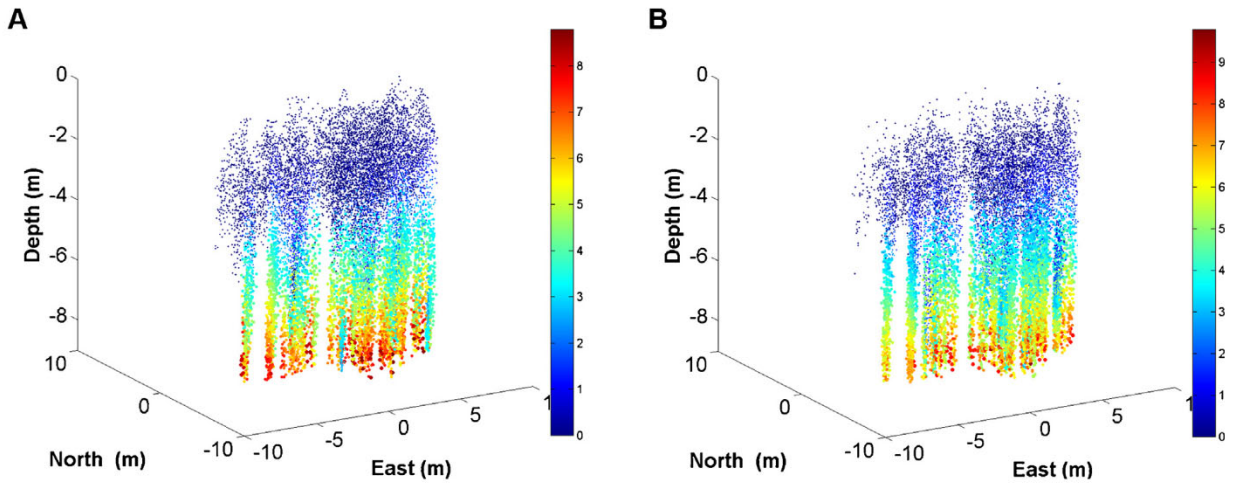
A

B

Fig. 6. The low tide bubble plume at the measured leakage rate, with the bubble diameter (mm) shown by both the colour map and the size of the marker. (A) Bubble plume prediction with no bubble interactions; (B) Bubble plume prediction with bubble breakup and coalescence interactions.
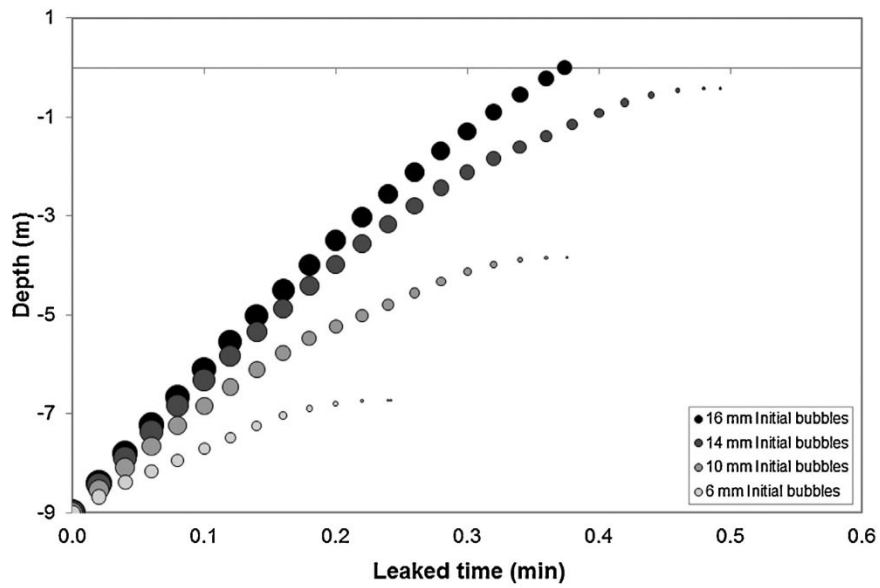

Fig. 7. Bubble dissolution at 9 m depth, showing individual bubbles with initial size >14 mm reaching the water surface (0 m depth) and leaking into the atmosphere.
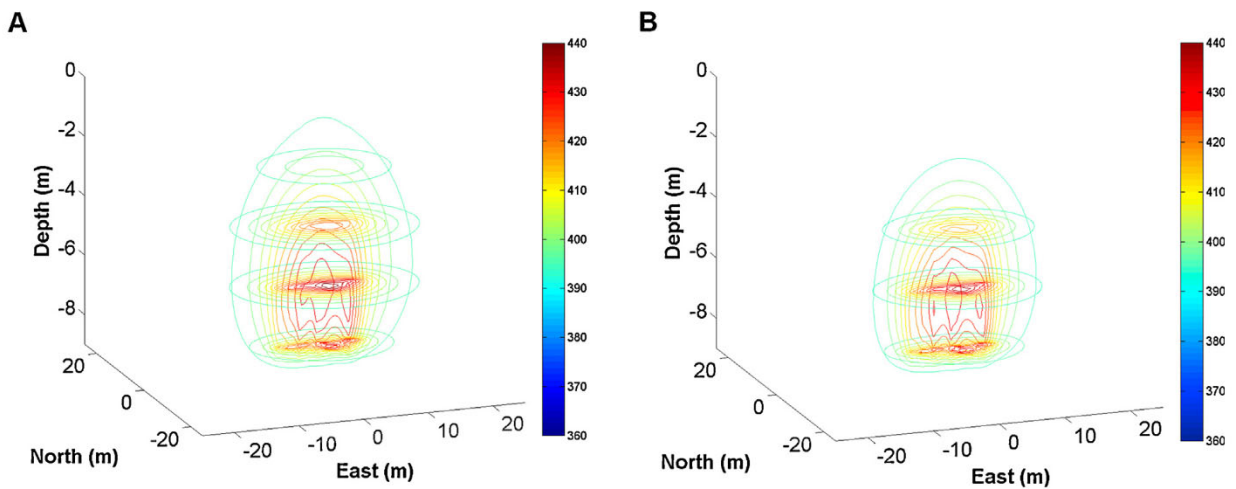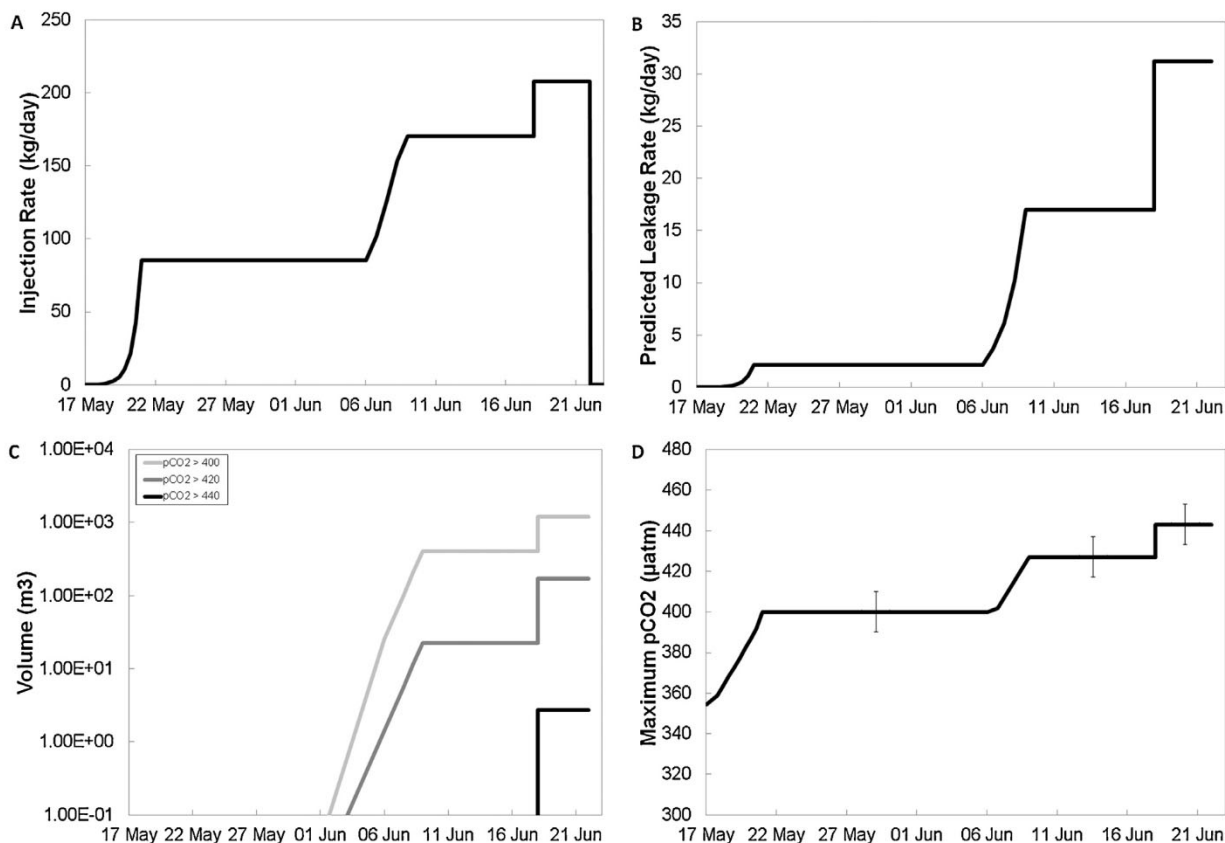
A

B

Fig. 8. Contours of low tide $p\mathrm{CO_2}$ (μatm) at the measured leakage rate and bubble sizes, shown at depths of 2, 4, 6 and 8 m. (A) Seawater plume with no bubble interactions; (B) seawater plume with bubble breakup and coalescence interactions.

Fig. 9. (A) QICS experiment CO_2 injection rate (kg/day); (B) predicted CO_2 leakage rate and injection rate into the model simulation (kg/day); (C) volume of pCO_2 from the simulation (m³); (D) maximum pCO_2 from the simulation (µatm).

where the leakage rates are predicted as 2.3 kg/day, 17.0 kg/day and 31.2 kg/day respectively as shown in Fig. 9. B). The simulations are performed step by step for each of the three leakage rates, by injecting CO_2 into the water column at the given leakage rate until the plumes develop to a semi-steady state, before increasing the rate to the next stage. In the first stage, leakage occurs from 10 pockmarks closest to the injection site, increasing to 25 pockmarks in the second stage moving in a south westerly direction, and up to 35 pockmarks at the final stage of the simulations as shown in Fig. 5. The results from the simulations are represented by the seawater volumes affected by a pCO_2 increase from background as seen in Fig. 9C, along with the maximum pCO_2 levels as seen in Fig. 9D.

As the injection rate increases during the QICS experiment, the leakage rate increases. The number of bubbles increases accordingly in order to maintain the bubble size distribution as seen in Eq. (2). This provides a greater interfacial area of the plume bubbles and seawater, enhancing the dissolution rate and generating larger volumes of pCO_2 changes, shown in Fig. 9C, which in turn provides a greater maximum pCO_2 as shown in Fig. 9D.

The pCO_2 fluctuates with the tide by ±10 µatm, with a maximum pCO_2 in the first 20 days of 400 µatm, increasing to 427 µatm when the injection rate is increased to 170 kg/day, and 443 µatm at the injection rate of 208 kg/day. In comparison with the observation data (Blackford, 2014) with the pCO_2 varying between 390 µatm and 1500 µatm in the high injection stages, it has to be realised that the flux where the measurement was taking place should be greater than predicted from the experiment observations, ~15% of total injections (Blackford, 2014). This can be due to the changes in activity across the pockmarks during the release period, although 35 pockmarks are active across the large leakage rate timeframe, they are not all active at the same time, and some are more active than others causing greater pCO_2 concentrations.

### 5.3. The prediction of impacts from considering a larger leakage rate to the seawater

With an increased leakage rate (the leakage rate is increased to 100% of the injection rate at 208 kg/day), a denser bubble plume is produced, with a far greater number of bubbles, and the maximum initial sizes of 9.8 mm again dominating at the leakage site as shown in Fig. 10A. Bubbles in such a dense plume, rise faster at a larger absolute velocity due to the bubble plume generating a vertical movement of seawater, and dissolve at a relatively low rate once steady state being reached due to the large surrounding concentration of CO_2 in the plume with the lack of unsaturated water. This coupling mechanism leads to the bubble plume reaching the water surface, as shown in Fig. 10A. Unlike in the more dilute bubble plume in the leakage rate experienced in the experiment where, the bubbles with the same 9.8 mm maximum size, only partially rises to the surface at low tide (Fig. 6), therefore it can be identified that the fate of the dense bubble plumes are significantly different with the fate of an individual bubble alone.

The impacts of a leakage of 100% of the experiment injection rate are more significant, with a maximum pCO_2 of 713 µatm as shown in Fig. 10B. To further investigate this effect, both the volumes of pCO_2 in the surrounding waters, and the vertical distribution of pCO_2 directly above the leakage source are measured and compared to those experienced in the QICS experiment simulations, the results are given in Fig. 11.

The volumes of seawater with a given pCO_2 changes, in addition to the maximum change in pCO_2 may be one parameter to assess the impacts of leaked CO_2 on marine environment. Such a volume is created by the coupling dynamics of CO_2 bubble plume and the ocean turbulence. As can be seen in Fig. 10B, for the 100% of injection leakage scenario at a steady state, the maximum pCO_2 changes only
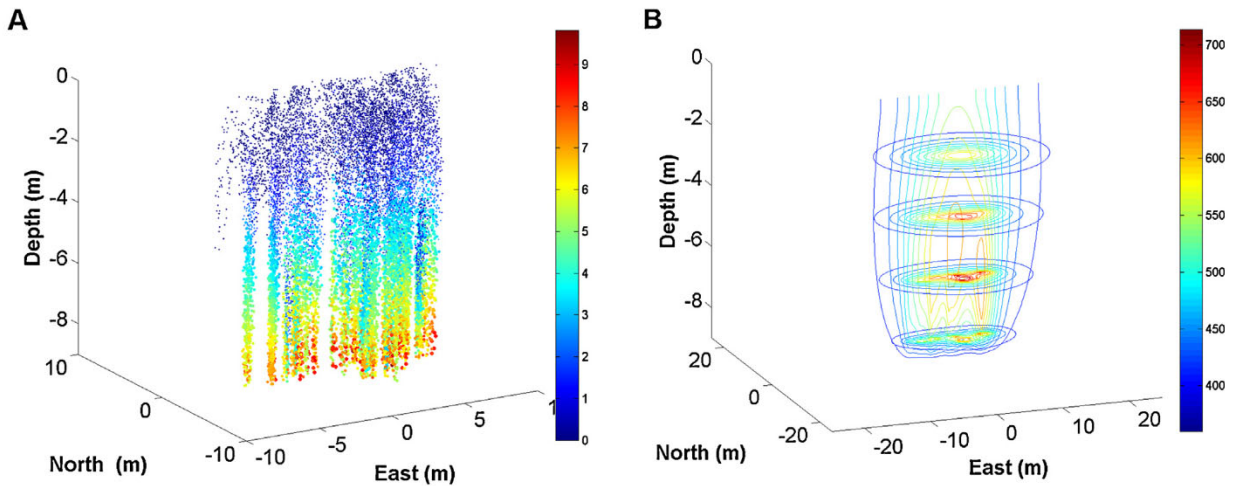
Fig. 10. (A) A low tide bubble plume at 208 kg/day leakage rate, with the bubble diameter (mm) shown by both the colour map and the size of the marker; (B) a low tide seawater pCO_2 (µatm) plume at 208 kg/day leakage rate, with contours of pCO_2 shown at depths of 2, 4, 6 and 8 m prediction.
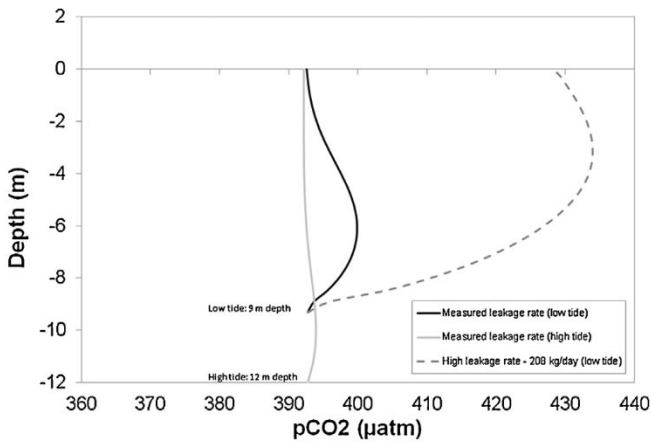
**Fig. 11.** The vertical profile of the mean pCO_2 (µatm) directly above the leakage pockmarks in a 625 m² area for each of the four case studies.

occur directly above the leakage area. However, the volumes in which the pCO_2 reaches 500, 600 and 700 µatm are found to be 685, 112 and 0.65 m³ respectively. From these results, it can be identified that the impacts on the marine environment are likely to remain in such a location if the leak continues into the ocean. In the point of view of monitoring and detecting the leakage, the

results provide the data that the changes in pCO_2 seem to be a parameter that is difficult to detect because of the relative small changes and spatial dimensions (volumes) associated with, which requires monitoring equipment with high resolution and having been strategically positioned.

Another parameter to measure the leakage impact is the vertical profile of the horizontal mean pCO_2 directly above the leakage pockmarks. In this study, the horizontal mean pCO_2 in a 625 m² area of pockmarks is predicted and demonstrated in Fig. 11. The simulation of the experiment at low tide provides a peak mean pCO_2 of 400 µatm a few metres above the leakage area. The high tide provides a lower leakage rate and therefore far less effect on the environment is experienced, with the greatest mean pCO_2 directly above the leakage location of 393 µatm. In contrast, the results from the leakage of full injection rate during the low tide where all the injected gas would leak to the water column, the greatest mean pCO_2 increases to 434 µatm directly 2 m above the leakage pockmark area.

The development and the structure of CO_2 solution plumes determine the highest change in pCO_2 and its location, which are the key parameters to assess the local impacts on marine environments. The highest changes in pCO_2 were expected to be on the seafloor (Dewar et al., 2013a) as seen in leakages in the deep ocean with relative large leak flux. However as the leakage rate increases, the greatest change is found from the simulations at the location a metre or two above the leakage pockmarks of the experiment in
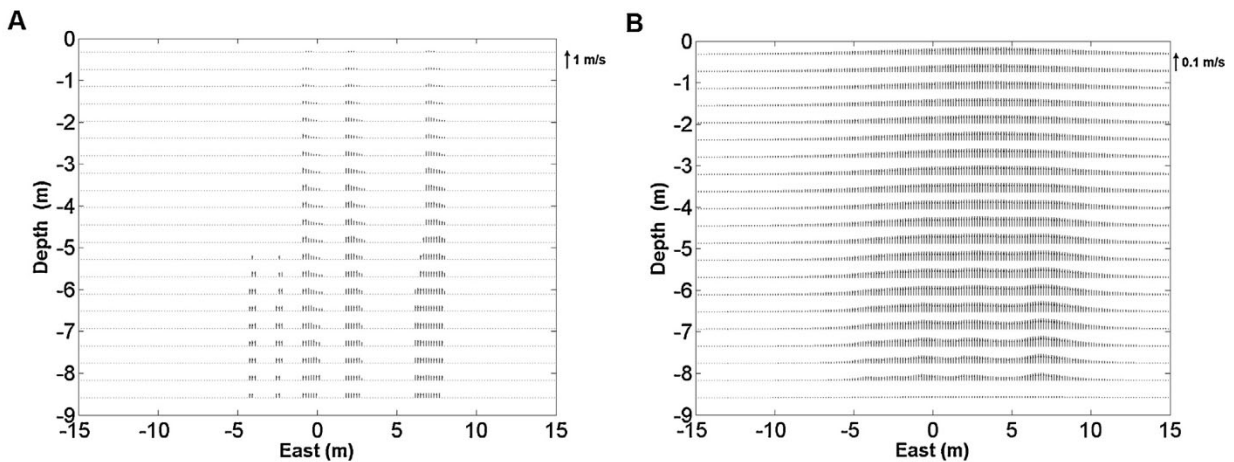
Fig. 12. Relative velocity vectors of plumes at a vertical cross-section of bubble plume in the 208 kg/day case study. (A) Bubble plume; (B) dissolved CO_2 solution plume.

the shallow water. What is also noticed, as well, is that the CO_2 solution plume rises far higher than the bubble plume (Fig. 10). This is investigated by the simulations and found that the momentum from the rising bubble plume is transferred to the seawater shown by the relative velocity of bubble plume in Fig. 12A, providing a greater upwards force than the negative buoyancy force from the increased density of the CO_2 solution, demonstrated by the velocities of CO_2 solution plumes in Fig. 12B. Such a plume development and structure are different with those from deep ocean. At larger leakage rates from deep ocean floor, the CO_2 solution plume would peel away from the bubble/droplet plume, as identified by laboratory experiments (Adams et al., 1993), where large CO_2 concentrations, due to the larger solubility of CO_2 into the water, lead to the gravitational effects dominating.

6. Discussion and conclusions

The dynamics of rising CO_2 bubbles in the Scottish seawater are investigated experimentally and through numerical modelling within the QICS project, Chen et al. (2005b) suggest that it may be possible to neglect interactions for bubbly flow due to weak interactions and a low range of distribution in bubble sizes. However the experimental results found during the QICS project showed multiple bubble interactions and a larger range of bubble size distribution, even within a low void fraction and low current bubbly flow, proving the need to investigate further. This need has been confirmed by the inclusion of interaction sub-models in simulations, which although have a minor effect on the maximum and mean bubble sizes, do have an effect on the distribution of bubble sizes and shapes, which in turn affect the dissolution rate of bubbles and the structure of the dissolved CO_2 plume.

The simulations with interactions bring the bubble rise heights closer to that observed from the experiment, where some bubbles were found to reach the surface. A greater range of bubble sizes from other pockmarks than those from three recorded are suggested from the plume and individual bubble simulations.

To predict the observation data and mean pCO_2 over the leakage zone, it is suggested that the full injection rate of 208 kg/day is required due to the leakage mechanism experienced at the end of the injection. Even though only 15% of the CO_2 is leaked as bubbles being observed from selected pockmarks, the surrounding sediments around the leakage chimney could be approaching a saturated state. The effect of this is, when the injection rate is increased, a faster migration of the CO_2 through the chimney will be experienced. This could allow 100% of the CO_2 to leak to the water column, providing the pCO_2 in the simulations of 713 μatm. This is lower than the peak recorded within the experiment of 1500 μatm although is approaching the mean pCO_2 across the time frame of 740 μatm. This could be explained through the following suggested situations, the first is that although there are 35 pockmarks of gas being released as shown in Fig. 5, not all pockmarks were leaking at the same time, they also do not have an even distribution of leakage rate, meaning some pockmarks are more active than others, which provides a greater concentration of pCO_2. The other possibility is that, as the leakage rate increased, the strong bubble steams force the saturated brine from the sediments erupting to the seawater, increasing the pCO_2 to the peak levels of 1500 μatm close to the seafloor, before settling back down at between 400 and 700 μatm. The simulation results for the high tide case, show the pCO_2 level of 390 μatm matches the observation data from the experiment, until the point where the leakage rate is increased, which partially supports these two suggested explanations.

The simulations, and the related data from the QICS experiment, are both of a small scale in time frame and spatial dimensions for the leakage from shallow seawater relative to the majority of the oceans. However, the results can be of reference with investigations of the assessment and monitoring of CO_2 leakage from depth down to about 400 m, at which depth the CO_2 is in the gas phase.

Nesting the small scale plume model to larger scale models, such as the Oceanic General Circulation Model (OGCM), may provide buffering through dilution and dispersion over a far longer period of time in the larger, meso/regional and global scales, including transportation into deeper waters and surface water to air CO_2 exchange may be simulated. This integrated model system allows the overall prediction of the biological impact in large-scale under seabed carbon sequestration in the ocean in the small, regional and global scale over related timeframes. An issue that does however also need further investigation is with such a shallow leak, how large localised concentrations affect the water–air surface mass transfer directing dissolved CO_2 to the atmosphere (the second leakage), along with the effect of the topography on the development of the plumes.

Acknowledgements

References

Adams, E.E., Golomb, D., Zhang, X.Y., Herzog, H.J., 1993. Confined release of CO_2 into shallow seawater. In: The Second International Workshop on Interaction between CO_2 and Ocean, Tsukuba, Japan.

Alendal, G., Drange, H., 2001. Two-phase, near-field modeling of purposefully released CO_2 in the ocean. J. Geophys. Res.: Oceans 106 (C1), 1085–1096.

Blackford, J.C., Stahl, H., Bull, J.M., Berges, B.J.P., Cevatoglu, M., Lichtschlag, A., Connelly, D., James, R.H., Kita, J., Long, D., Naylor, M., Shitashima, K., Smith, D., Taylor, P., Wright, I., Akhurst, M., Chen, B., Gernon, T.M., Hauton, C., Hayashi, M., Kaieda, H., Leighton, T.G., Sato, T., Sayer, M.D.J., Suzumura, M., Tait, K., Vardy, M.E., White, P.R., Widdicombe, S., 2014. Detection and impacts of leakage from sub-seafloor Carbon Dioxide Storage. Nat. Clim. Changes 4, 1011–1016, http://dx.doi.org/10.1038/nclimate2381.

Bozzano, G., Dente, M., 2001. Shape and terminal velocity of single bubble motion: a novel approach. Comput. Chem. Eng. 25 (May (4–6)), 571–576.

Bradshaw, P., Huang, G.P., 1995, October. The law of the wall in turbulent flow. Proc. R. Soc. Lond. 451, 165–188.

Chen, B., Song, Y., Nishio, M., Akai, M., 2003. Large-eddy simulation of double-plume formation induced by CO_2 dissolution in the ocean. Tellus B 55 (2), 723–730.

Chen, B., et al., 2005a. Modeling near-field dispersion from direct injection of carbon dioxide into the ocean. J. Geophys. Res.: Oceans 110 (C09S15).

Chen, P., Sanyal, J., Duduković, M.P., 2005b. Numerical simulation of bubble columns flows: effect of different breakup and coalescence closures. Chem. Eng. Sci. 60 (February (4)), 1085–1101.

Cheung, S.C.P., Yeoh, G.H., Tu, J.Y., 2007. On the modelling of population balance in isothermal vertical bubbly flows – average bubble number density approach. Chem. Eng. Process.: Process Intensif. 46 (August (8)), 742–756.

Coulaloglou, C.A., Tavlarides, L.L., 1977. Description of interaction processes in agitated liquid–liquid dispersions. Chem. Eng. Sci. 32 (11), 1289–1297.

Dewar, M., Wei, W., McNeil, D., Chen, B., 2013a. Small-scale modelling of the physiochemical impacts of CO_2 leaked from sub-seabed reservoirs or pipelines within the North Sea and surrounding waters. Mar. Pollut. Bull. 73 (August (2)), 504–515.

Dewar, M., Wei, W., McNeil, D., Chen, B., 2013b. Simulation of the near field physiochemical impact of CO_2 leakage into shallow water in the North Sea. Energy Proc. 37, 3413–3423.

Fu, X.Y., Ishii, M., 2002. Two-group interfacial area transport in vertical air–water flow – II. Model evaluation. Nucl. Eng. Des. 219 (February (2)).

Gibson, R.N., Atkinson, R.J.A., Gordon, J.D.M., 2011. Oceanography and Marine Biology: An Annual Review. CRC Press, s.l.

Greene, C.A., Wilson, P.S., 2012. Laboratory investigation of a passive acoustic method for measurement of underwater gas seep ebullition. J. Acoust. Soc. Am. 131, EL61–EL66.

Hibiki, T., Ishii, M., 2000a. One-group interfacial area transport of bubbly flows in vertical round tubes. Int. J. Heat Mass Transf. 43 (August (15)), 2711–2726.

Hibiki, T., Ishii, M., 2000, November. Two-group interfacial area transport equations at bubbly-to-slug flow transition. Nucl. Eng. Des., 39–76.

Hibiki, T., Ishii, M., 2002. Development of one-group interfacial area transport equation in bubbly flow systems. Int. J. Heat Mass Transf. 45 (May (11)), 2351–2372.

IEA Greenhouse Gas R&D Programme, 2008. Assessment of Sub Sea ecosystem impacts, August.

Ishii, M., Kim, S., 2001. Micro four-sensor probe measurement of interfacial area transport for bubbly flow in round pipes. Nucl. Eng. Des. 205 (March (1–2)), 123–131.

Ishii, M., Mishima, K., 1980. Study of two-fluid model and interfacial area. In: Argonne National Laboratory Report ANL-80-111. (NUREG/CR-1873).

Ito, M., 1984. Chemical Handbook, third ed. The Chemical Society of Japan, Tokyo, s.l.: Maruzen Publishing Company.

Kano, Y., et al., 2009. Model prediction on the rise of pCO_2 in uniform flows by leakage of CO_2 purposefully stored under the seabed. Int. J. Greenh. Gas Control 3 (September (5)), 617–625.

Levich, V.G., 1962. Physiochemical Hydrodynamics. Prentice-Hall, Englewood Cliffs, NJ, USA.

Luo, H., Svendsen, H.F., 1996. Theoretical model for drop and bubble breakup in turbulent dispersions. AIChE J. 42 (5), 1225–1233.

Nguyen, V.-T., Song, C.-H., Bae, B.-U., Euh, D.-J., 2013, September. Modeling of bubble coalescence and break-up considering turbulent suppression phenomena in bubbly two-phase flow. Int. J. Multiphase Flow 54, 31–42.

Oolman, T.O., Blanch, H.W., 1986a. Bubble coalescence in air-sparged bioreactors. Biotechnol. Bioeng. 28 (4), 578–584.

Oolman, T.O., Blanch, H.W., 1986b. Bubble coalescence in stagnant liquids. Chem. Eng. Commun. 43 (4–6), 237–261.

Prince, M.J., Blanch, H.W., 1990. Bubble coalescence and break-up in air-sparged bubble columns. AIChE J. 36 (10), 1485–1499.

Sato, T., Sato, K., 2002. Numerical prediction of the dilution process and its biological impacts. J. Mar. Sci. Technol. 6 (4), 169–180.

Sellami, N., Dewar, M., Stahl, H., 2015. Dynamics of rising CO_2 bubble plumes in the QICS field experiment. Part 1 – The experiment. Int. J. Greenh. Gas Control 38, 52–63.

Song, Y., Chen, B., Nishio, M., Akai, M., 2005. The study on density change of carbon dioxide seawater solution at high pressure and low temperature. Energy 30 (11–12), 2298–2307.

Sun, X., Kim, S., Ishii, M., Beus, S.G., 2004. Modeling of bubble coalescence and disintegration in confined upward two-phase flow. Nucl. Eng. Des. 230 (May (1–3)), 3–26.

Unesco, 1981. Tenth report of the joint panel on oceanographic tables and standards. Unesco Technical Papers in Marine Science, vol. 36., pp. 24–29.

Wu, Q., Kim, S., Ishii, M., Beus, S.G., 1998. One-group interfacial area transport in vertical bubbly flow. Int. J. Heat Mass Transf. 41 (8–9), 1103–1112.

Yao, W., Morel, C., 2004. Volumetric interfacial area prediction in upward bubbly two-phase flow. Int. J. Heat Mass Transf. 47 (January (2)), 307–328.

Zhao, L., Boufadel, M.C., Socolofsky, S.A., Adams, E., King, T., Lee, K., 2014. Evolution of droplets in subsea oil and gas blowouts: development and validation of the numerical model VDROP-J. Mar. Pollut. Bull. 83 (June (1)), 58–69, http://dx.doi.org/10.1016/j.marpolbul.2014.04.020, ISSN 0025-326X.

Zheng, L., Yapa, P.D., 2002. Modeling gas dissolution in deepwater oil/gas spills. J. Mar. Syst. 31 (January (4)), 299–309.